OCCAM

OXFORD CENTRE FOR COLLABORATIVE APPLIED MATHEMATICS

Report Number 11/62

Neural field model of binocular rivalry waves

by

Paul C. Bressloff and Matthew Webber

Neural field model of binocular rivalry waves

Abstract We present a neural field model of binocular rivalry waves in visual cortex. For each eye we consider a one–dimensional network of neurons that respond maximally to a particular feature of the corresponding image such as the orientation of a grating stimulus. Recurrent connections within each one-dimensional network are assumed to be excitatory, whereas connections between the two networks are inhibitory (cross-inhibition). Slow adaptation is incorporated into the model by taking the network connections to exhibit synaptic depression. We derive an analytical expression for the speed of a binocular rivalry wave as a function of various neurophysiological parameters, and show how properties of the wave are consistent with the wave–like propagation of perceptual dominance observed in recent psychophysical experiments. In addition to providing an analytical framework for study-ing binocular rivalry waves, we show how neural field methods provide insights into the mechanisms underlying the generation of the waves. In particular, we highlight the important role of slow adaptation in providing a "symmetry breaking mechanism" that allows waves to propagate.

1 Introduction

A number of phenomena in visual perception involve wave–like propagation dynamics. Examples include perceptual filling-in [14], migraine aura [18], expansion of illusory contours [17] and the line–motion illusion [21]. Another important example, which is the focus of this paper, is the wave–like propagation of perceptual dominance during binocular rivalry [41, 27, 22, 23]. Binocular rivalry is the phenomenon whereby perception switches back and forth between different images presented to the two eyes. The resulting fluctuations in perceptual dominance and suppression provide a basis for non-invasive studies of the human visual system and the identification of possible neural mechanisms under-

Paul C. Bressloff · Matthew Webber
Mathematical Institute, University of Oxford, 24-29 St. Giles', Oxford OX1 3LB, UK

Paul C. Bressloff
Department of Mathematics, University of Utah,
Salt Lake City, UT, 84112-0090
E-mail: bressloff@math.utah.edu

lying conscious visual awareness [6, 7]. One way to observe and measure the speed of perceptual waves in psychophysical experiments [41, 27] is to take the rival images to be a low–contrast radial grating presented to one eye and a high–contrast spiral grating presented to the other eye. Each image is restricted to an annular region of the visual field centered on the fixation point of the observer, thus effectively restricting wave propagation to the one dimension around the annulus. Switches in perceptual dominance can then be triggered using a brief rapid increase in stimulus contrast within a small region of the suppressed low-contrast grating. This induces a perceptual traveling wave in which the observer perceives the local dominance of the low–contrast image spreading around the annulus. The observer presses a key when the perceptual wave reaches a target area at a fixed distance from the trigger zone, and this determines the wave speed [41, 27]. Since the rival images consist of oriented gratings, one might expect that primary visual cortex (V1) plays some role in the generation of binocular rivalry waves. Indeed, it has been shown using functional magnetic resonance imaging that there is a systematic correspondence between the spatiotemporal dynamics of activity in V1 and the time course of perceptual waves [27]. However, it has not been established whether the waves originate in V1 or are evoked by feedback from extrastriate cortex.

Recently Kang *et. al.* [22, 23] have developed a new psychophysical method for studying binocular rivalry waves that involves periodic perturbations of the rival images. An observer tracks rivalry within a small, central region of spatially extended rectangular grating patterns, while alternating contrast triggers are presented repetitively in the periphery of the rival patterns. The basic experimental set up is illustrated in Fig. 1. A number of interesting results have been obtained from

these studies. First, over a range of trigger frequencies, the switching between rival percepts within the central regions is entrained to the triggering events. Moreover, the optimal triggering frequency depends on the natural frequency of spontaneous switching (in the absence of triggers). Second, the latency between triggering event and perceptual switching increases approximately linearly with the distance between the triggering site and the central region being tracked by the observer, consistent with the propagation of a traveling front. Third, the speed of the traveling wave across observers covaries with the spontaneous switching rate.

In this paper we analyze the existence and stability of binocular rivalry waves in a continuum neural field model of visual cortex. We derive an analytical expression for the wave speed as a function of neurophysiological parameters, and use this to show how our model reproduces various experimental results found by Kang *et al.* [22, 23], in particular, the observation that wave speed covaries with the natural alternation rate. Our model is essentially a continuum version of a previous computational model of rivalry waves based on a discrete two layer neural network [41, 23]. The two layers represent cortical neurons responsive to one or more features of the image presented to the left and right eye respectively. Such features could include the orientation of a spatially extended grating stimulus or distinguish between spiral and radial annulus patterns. In the discrete computational model, connections within a layer were taken to be excitatory, whereas neurons between layers mutually inhibited each other via a set of local interneurons. Moreover, in order to allow switching between the dominant and suppressed populations, the excitatory neurons were assumed to exhibit some form of slow spike frequency adaptation. In our neural field version of this model, we consider an alternative form of slow adaptation based on
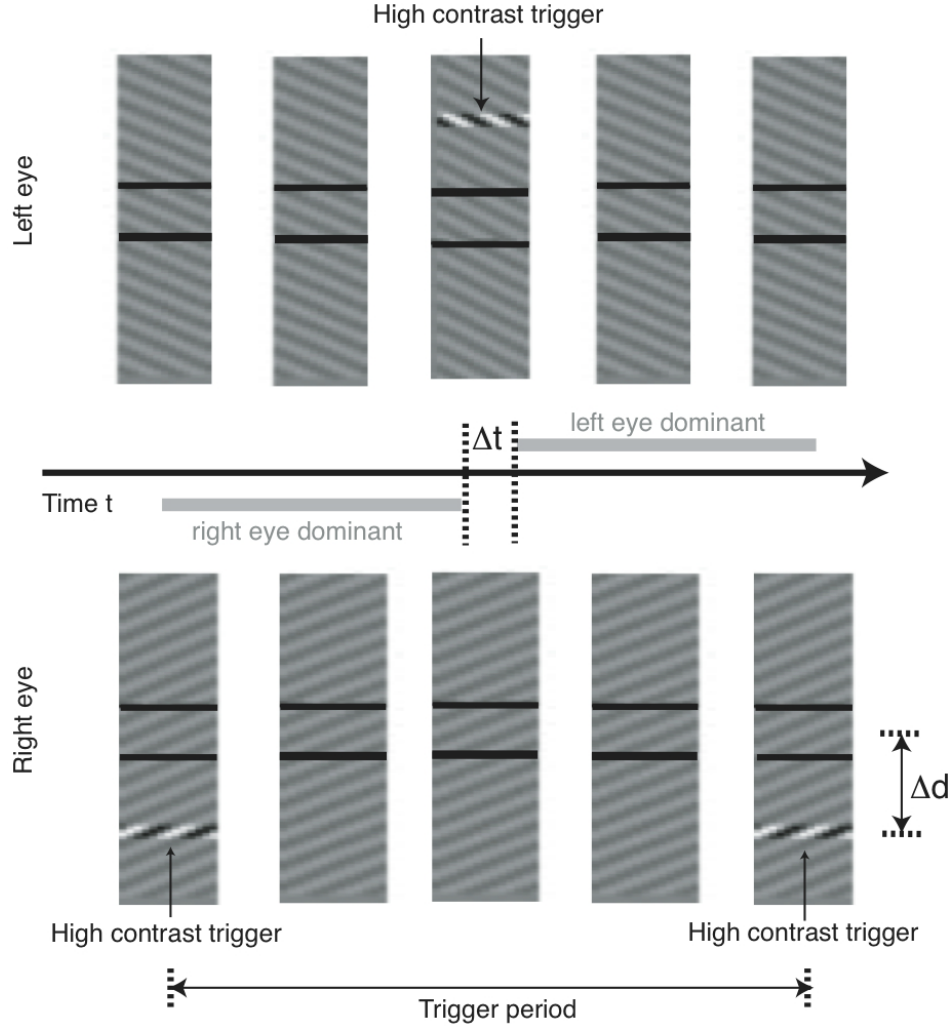
Fig. 1 Schematic diagram illustrating experimental prototocol used to study binocular rivalry waves [22]. High contrast triggers are presented periodically in antiphase within the upper extended region of one grating pattern and within the lower region of the rival pattern. Subject simply reports perceptual alternations in rival dominance within the central monitoring region indicated by the horizontal black lines on each pattern. The monitoring region is a distance Δd from the trigger region, which can be adjusted. If Δt is the latency between the triggering event and the subsequent observation of a perceptual switch, then the speed c of the wave is given by the slope of the plot $\Delta d = c\Delta t$.

depressing synapses. In addition to providing an analytical framework for studying binocular rivalry waves, we show how neural field methods provide insights into the mechanisms underlying the generation of the waves. In particular, we highlight the important role of slow adaptation in providing a "symmetry breaking mechanism" that allows fronts to propagate.

2 The Model

In order to model binocular rivalry waves in the presence of oriented grating stimuli [41, 22, 23], it

is useful to review some of the stimulus response properties of neurons in the primary visual cortex (V1) [19, 20]. First, each neuron in V1 responds to light stimuli in a restricted region of the visual field called its *classical receptive field*; stimuli outside a neuron's receptive field do not directly affect its activity. Second, most neurons in V1 respond preferentially to stimuli targeting either the left or right eye, which is known as *ocular dominance*. It has been suggested that neurons with different ocular dominance may inhibit one another if they have nearby receptive fields [24]. Third, most neurons in V1 are tuned to respond maximally when a stimulus of a particular orientation is in their receptive field [19, 8]. This is known as a neuron's *orientation preference*, and the neuron will not respond if a stimulus is sufficiently different from its preferred orientation. Finally, multielectrode recordings and optical imaging have established that at each point in the visual field there exists a corresponding set of neurons spanning the entire spectrum of orientation preferences that are packed together as a unit in V1, known as a *hypercolumn* [20, 38, 8]. Within each hypercolumn, neurons with sufficiently similar orientations tend to excite each other whereas those with sufficiently different orientations inhibit each other, and this serves to sharpen a particular neuron's orientation preference [5, 15]. Moreover, anatomical evidence suggests that inter-hypercolumn connections link neurons with similar orientation preferences [35, 3]. The functional relationship between stimulus feature preferences and synaptic connections within V1 thus suggests that V1 is a likely substrate of simple examples of binocular rivalry such as those involving sinusoidal grating stimuli.

Binocular rivalry waves consist of two basic components: the switching between rivalrous left/right eye states and the propagation of the switched state across a region of cortex. Let us first focus on the switching mechanism by neglecting spatial effects. Suppose that distinct oriented grating patterns are presented to the two eyes such as those shown in Fig. 1. This induces rivalry due to the combination of orientation specific and ocular dominant cross-inhibition in V1 [5, 35, 7]. During left eye stimulus dominance, it is assumed that a group of the left eye neurons that respond to vertical orientations are firing persistently, while right eye neurons are suppressed by cross-inhibitory connections. Following this, some slow adaptive process such as synaptic depression or spike frequency adaptation causes a switch so that right eye neurons tuned to the oblique orientation fire persistently, suppressing the left eye neurons. The cycle of left eye neural dominance along with right eye neural suppression followed by right eye neural dominance along with left eye neural suppression can then repeat itself in the form of rivalrous oscillations. This basic model of reciprocal inhibition paired with a slow adaptive process has often been used to phenomenologically model the neural substrate of binocular rivalry oscillations [16, 34, 41, 26, 37, 32, 33, 25].

In order to take into account the propagation of activity seen in binocular rivalry waves [41, 22, 23], we will consider a continnuum neural field model. Several previous studies have modeled the spontaneous switching between rivalrous oriented stimuli in terms of a pair of ring networks (neural fields on a periodic domain) with slow adaptation and cross-inhibition, representing a pair of hypercolumns for the left and right eyes, respectively [26, 25]. In these models, the rivalrous states consist of stationary activity bumps coding for either the left or right eye stimuli. (Rivalry effects in a spatially extended model have also been examined in a prior study by Loxley and Robinson [28], in which rivalrous stimuli are presented to a single one–dimensional network). However, these models were not used to study binocular rivalry waves and, as formu-
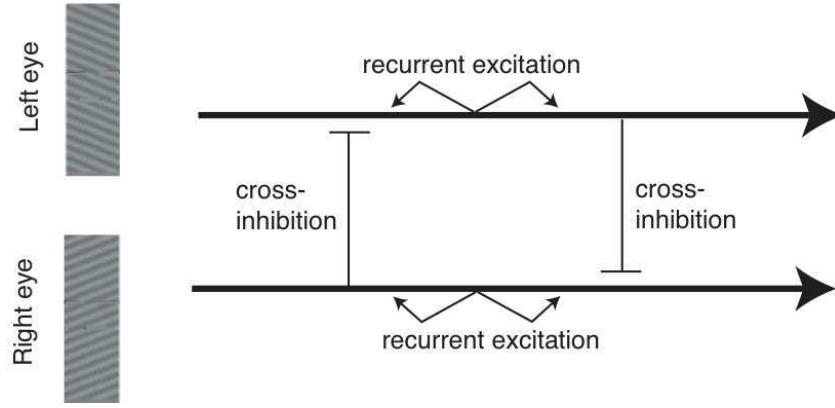
Fig. 2 Schematic diagram of network architecture consisting of two one–dimensional neural fields. Suppose that the left eye is shown a 135 degree grating and the right eye is shown a 45 degree grating. Then one of the neural fields represents the activity of neurons tuned to 135 degree orientations in the left eye, whilst the other neural field represents the activity of neurons tuned to 45 degree orientations in the right eye. Recurrent connections within each one-dimensional network are assumed to be excitatory, whereas connections between the two networks are inhibitory (cross-inhibition). The excitatory and inhibitory weight distributions are taken to be Gaussians. Slow adaptation is incorporated into the model by taking the network connections to exhibit synaptic depression.

lated, were on the wrong spatial scale since they only considered short–range spatial scales comparable to a single hypercolumn. One way to proceed would be to construct a more general coupled ring model along the lines of Bressloff *et. al.* [10, 11], in which two sets of hypercolumns (ring networks) are distributed along a pair of lines corresponding to the left and right eyes, respectively, such that along each line the synaptic weights can be decomposed into short-range intra-columnar interactions and long–range inter-columnar interactions, together with cross-inhibitory connections between the left and right eye networks. In this paper, we will consider a simpler network architecture in which we neglect the internal structure of a hypercolumn. That is, for each eye we consider a one–dimensional network of neurons whose orientation preference coincides with the orientation of the corresponding grating stimulus, which is a reasonable first approximation from the perspective of the experiments conducted by Kang *et. al.* [22, 23]. Recurrent connections within each one-

dimensional network are assumed to be excitatory, whereas connections between the two networks are inhibitory (cross-inhibition). Slow adaptation is incorporated into the model by taking the network connections to exhibit synaptic depression along the lines of Kilpatrick and Bressloff [25]. The basic architecture is shown schematically in Fig. 2. Note that a similar network architecture was previously considered in a computational model of binocular rivalry waves [41, 27], in which cross inhibition was mediated explicitly by interneurons and, rather than including depressing synapses, the excitatory neurons were taken to exhibit spike frequency adaptation. The most significant difference between our approach and the computational approach is that the latter considers a discrete neural network rather than a continuum neural field. As we will establish in this paper, one advantage of neural field theory is that analytical methods can be used to derive conditions for the existence and stability of traveling waves, and to derive formulae

relating the wave speed to various neurophysiological parameters.

Let $u(x,t)$ and $v(x,t)$ denote the activity of the left and right eye networks at position $x \in \mathbb{R}$ at time t. The associated neural field equations are taken to be of the form

$$\tau \frac{\partial u(x,t)}{\partial t} = -u(x,t) + I_u(x,t) \tag{2.1a}$$

$$+ \int_{-\infty}^{\infty} w_e(x-x')q_u(x',t)f(u(x',t)))dx'$$

$$- \int_{-\infty}^{\infty} w_i(x-x')q_v(x',t)f(v(x',t)))dx'$$

$$\tau_s \frac{\partial q_u(x,t)}{\partial t} = 1 - q_u(x,t) - \beta q_u(x,t)f(u(x,t)), \tag{2.1b}$$

and

$$\tau \frac{\partial v(x,t)}{\partial t} = -v(x,t) + I_v(x,t) \tag{2.2a}$$

$$+ \int_{-\infty}^{\infty} w_e(x-x')q_v(x',t)f(v(x',t)))dx'$$

$$- \int_{-\infty}^{\infty} w_i(x-x')q_u(x',t)f(u(x',t)))dx',$$

$$\tau_s \frac{\partial q_v(x,t)}{\partial t} = 1 - q_v(x,t) - \beta q_v(x,t)f(v(x,t)). \tag{2.2b}$$

The nonlinear function f represents the mean firing rate of a local population and is usually taken to be a smooth, bounded monotonic function such as a sigmoid

$$f(u) = \frac{1}{1 + e^{-\eta(u-\kappa)}}, \tag{2.3}$$

with gain η and threshold κ. However, in order to derive explicit traveling wave solutions, it will be convenient to consider the high gain limit $\eta \to \infty$ of (2.3) such that f becomes a Heaviside function [2, 30, 13]

$$f(u) = H(u-\kappa) = \begin{cases} 0 \text{ if } u < \kappa \\ 1 \text{ if } u > \kappa. \end{cases} \tag{2.4}$$

The distribution w_e of excitatory connections between neurons of the same eye preference and the distribution of cross-inhibitory connections between neurons of the opposite eye preference are both taken to be Gaussians:

$$w_e(r) = \frac{a_e}{\sqrt{2\pi\sigma_e^2}} e^{-\frac{r^2}{2\sigma_e^2}}, \quad w_i(r) = \frac{a_i}{\sqrt{2\pi\sigma_i^2}} e^{-\frac{r^2}{2\sigma_i^2}} \tag{2.5}$$

We assume that excitatory connections are longer range than inhibitory connections, $\sigma_e > \sigma_i$ and fix length scales by setting $\sigma_e = 2$ and $\sigma_i = 1$ at baseline. We expect excitatory connections to span a cortical hypercolumn so that σ_e will be of the order 200 μm. We also fix the temporal scale of the network by setting the membrane time constant $\tau = 1$; the membrane time constant is typically around 10msec. Depressing synapses are incorporated into the model in the form of the presynaptic scaling factors q_u, q_v evolving according to equations (2.1b) and (2.2b). These scaling factors can be interpreted as a measure of available presynaptic resources, which are depleted at a rate proportional to $\beta q f$ [39, 36, 4], and are recovered on a timescale specified by the constant τ_s. Specifically, we will study the effect of slow short term synaptic depression (experimentally shown to recover over 5-10s [40, 12]). Slow short term synaptic depression has been implicated as a mechanism for contrast adaptation in V1, due to its comparable recovery timescale of 5-10s [40]. Thus, there is evidence for participation of this slower depression in processes of V1 in addition to faster short term synaptic depression, which recovers on timescales of roughly 200-800ms [1, 40]. Finally, we take I_u, I_v to represent the effective strength of the left and right eye stimuli, respectively. Recall that we are only modeling neurons whose orientation preference coincides with the corresponding stimulus orientation so that we can take the unperturbed network to have constant homogeneous inputs. (The induction of traveling waves requires locally perturbing one of the inputs).

3 Travelling Waves

3.1 Non-depressing synapses ($\beta = 0$)

In our simplified model, we interpret the binocular rivalry wave seen in the experiments of Kang *et. al.* [22, 23] as a traveling wave front solution of the neural field equations (2.1) and (2.2), in which a high activity state invades the suppressed left eye network, say, whilst retreating from the dominant right eye network. Let us begin by ignoring the effects of synaptic depression, that is, we set $\beta = 0$ and $q_u = q_v \equiv 1$. We also assume that both inputs have the same strength or contrast so that $I_u = I_v = I$. We then obtain the reduced system of equations (for $\tau = 1$ and f given by the Heaviside (2.4))

$$\frac{\partial u}{\partial t} + u = \int_{-\infty}^{\infty} w_e(x - x')H(u(x', t) - \kappa)dx'$$
$$- \int_{-\infty}^{\infty} w_i(x - x')H(v(x', t) - \kappa)dx' + I,$$
$$(3.1)$$

and

$$\frac{\partial v}{\partial t} + v = \int_{-\infty}^{\infty} w_e(x - x')H(v(x', t) - \kappa)dx'$$
$$- \int_{-\infty}^{\infty} w_i(x - x')H(u(x', t) - \kappa)dx' + I.$$
$$(3.2)$$

Given that the differential operator $D = \frac{\partial}{\partial t} + 1$ has a Green's function given by $G(t, s) = \eta(t - s)$ with

$$\eta(t) = \begin{cases} 0 & t < 0 \\ e^{-t} & t > 0, \end{cases}$$

we can re-write the above equations in purely integral form:

$$u(x, t) = I + \int_0^{\infty} \eta(s)G_e[u](x, t - s)ds$$
$$- \int_0^{\infty} \eta(s)G_i[v](x, t - s)ds \qquad (3.3)$$

$$v(x, t) = I + \int_0^{\infty} \eta(s)G_e[v](x, t - s)ds$$
$$- \int_0^{\infty} \eta(s)G_i[u](x, t - s)ds \qquad (3.4)$$

where

$$G_p[u](x, t) = \int_{-\infty}^{\infty} w_p(y)H(u(x - y, t) - \kappa)dy$$
$$(3.5)$$

for $p = e, i$.

Homogeneous fixed point solutions (U^*, V^*) of equations (3.3) and (3.4) satisfy the pair of equations

$$U^* = \overline{w}_e H(U^* - \kappa) - \overline{w}_i H(V^* - \kappa) + I$$
$$V^* = \overline{w}_e H(V^* - \kappa) - \overline{w}_i H(U^* - \kappa) + I,$$

where

$$\overline{w}_e = \int_{-\infty}^{\infty} w_e(x)dx, \quad \overline{w}_i = \int_{-\infty}^{\infty} w_i(x)dx. \qquad (3.6)$$

There are a maximum of four possible fixed point solutions, all of which are stable. First, there is the off state $U^* = V^* = I$, which occurs when $I < \kappa$, that is, the input is not strong enough to directly activate either population. Second there is the on-state or fusion state $U^* = V^* = \overline{w}_e - \overline{w}_i + I$, which occurs when $I > \kappa + \overline{w}_i - \overline{w}_e$. This case is more likely when recurrent excitation is strong or cross-inhibition is weak. Finally, there are two winner–take–all (WTA) states in which one population dominates the other: the left eye dominant state $(U^*, V^*) = \mathbf{X}_L \equiv (\overline{w}_e + I, I - \overline{w}_i)$ and the right eye dominant state $(U^*, V^*) = \mathbf{X}_R \equiv (I - \overline{w}_i, \overline{w}_e + I)$. These states exist when $I > \kappa - \overline{w}_e$ and $I < \kappa + \overline{w}_i$. We will assume that the space–clamped network operates in a regime where the WTA fixed points exist.

Let us now consider a traveling wave front solution of the form

$$u(x, t) = U(x - ct), \quad v(x, t) = V(x - ct)$$

where c is the wave speed and $\xi = x - ct$ is a traveling wave coordinate. We assume that

$(U(\xi), V(\xi)) \to \mathbf{X}_L$ as $\xi \to -\infty$,

$(U(\xi), V(\xi)) \to \mathbf{X}_R$ as $\xi \to \infty$

with $U(\xi)$ a monotonically decreasing function of ξ and $V(\xi)$ a montonically increasing function of ξ. It follows that if $c > 0$ then the wavefront represents a solution in which activity invades a supressed left eye network and retreats from a dominant right eye network. Substituting the traveling front solution into equations (3.3) and (3.4) gives

$$U(\xi) = I + \int_0^\infty \eta(s)\widehat{G}_e[U](\xi + cs)ds$$
$$- \int_0^\infty \eta(s)\widehat{G}_i[V](\xi + cs)ds$$

$$V(\xi) = I + \int_0^\infty \eta(s)\widehat{G}_e[V](\xi + cs)ds$$
$$- \int_0^\infty \eta(s)\widehat{G}_i[U](\xi + cs)ds.$$

where

$$\widehat{G}_p[U](\xi) = \int_{-\infty}^\infty w_p(y)H(U(\xi - y) - \kappa)dy, p = e, i$$

Given the asymptotic behavior of the solution and the requirements of monotonicity, we see that $U(\xi)$ and $V(\xi)$ each cross threshold at a single location, which may be different for the two eyes. Exploiting translation invariance we take $U(0) = \kappa$ and $V(\xi_0) = \kappa$. These threshold crossing conditions imply that the above equations simplify further according to

$$U(\xi) = \int_0^\infty \eta(s)\left[\int_{\xi+cs}^\infty w_e(y)dy\right.$$
$$\left. - \int_{-\infty}^{\xi-\xi_0+cs} w_i(y)dy\right]ds + I \qquad (3.7)$$

$$V(\xi) = \int_0^\infty \eta(s)\left[\int_{-\infty}^{\xi-\xi_0+cs} w_e(y)dy\right.$$
$$\left. - \int_{\xi+cs}^\infty w_i(y)dy\right]ds + I. \qquad (3.8)$$

It is convenient to introduce the function

$$\Psi_{\xi_0}(z) = \int_z^\infty w_e(y)dy - \int_{-\infty}^{z-\xi_0} w_i(y)dy. \qquad (3.9)$$

Exploiting the fact that the Gaussian weight distributions $w_e(y)$ and $w_i(y)$ are even functions of y, it can be seen that

$$\Psi_{\xi_0}(\xi_0 - z) = \int_{-\infty}^{z-\xi_0} w_e(y)dy - \int_z^\infty w_i(y)dy,$$

so that equations (3.7) and (3.8) can be rewritten in the more compact form

$$U(\xi) = \int_0^\infty \eta(s)\Psi_{\xi_0}(\xi + cs)ds + I \qquad (3.10)$$

$$V(\xi) = \int_0^\infty \eta(s)\Psi_{\xi_0}(\xi_0 - \xi - cs) + I. \qquad (3.11)$$

Finally, imposing the threshold conditions $U(0) = V(\xi_0) = \kappa$ gives

$$\kappa = \int_0^\infty \eta(s)\Psi_{\xi_0}(cs)ds + I, \qquad (3.12)$$

$$\kappa = \int_0^\infty \eta(s)\Psi_{\xi_0}(-cs)ds + I. \qquad (3.13)$$

It is now straightforward to show that a traveling front solution cannot exist for the neural field model without adaptation given by equations (3.1) and (3.2). For subtracting equation (3.13) from (3.12) implies that

$$\int_0^\infty \eta(s)\left[\Psi_{\xi_0}(cs) - \Psi_{\xi_0}(-cs)\right]ds = 0, \qquad (3.14)$$

which does not have a solution for any c, ξ_0 such that $c \neq 0$. The latter follows from equation (3.9), which shows that for $c \neq 0$,

$$c\left[\Psi_{\xi_0}(cs) - \Psi_{\xi_0}(-cs)\right]$$
$$= -c\int_{-cs}^{cs} w_e(y)dy - c\int_{-cs-\xi_0}^{cs-\xi_0} w_i(y)dy < 0$$

whereas $\eta(s) > 0$ for all $s \in [0, \infty)$. The non-existence of traveling fronts is consistent with the observation that in the absence of any cross-inhibition ($w_i \equiv 0$), the system reduces to two independent

one–dimensional neural fields with excitatory connections. In order to construct a front solution that simultaneously invades one network whilst retreating from the other we would require a one–dimensional excitatory neural field to be able to support a pair of counter-propagating front solutions with speeds $\pm c$, which is not possible [2]. Therefore, some mechanism must be introduced that breaks the exchange symmetry of the two one–dimensional networks. This cannot be achieved simply by taking $I_u \neq I_v$, since binocular rivalry waves are still observed when the left and right eye stimuli have the same contrast. An alternative approach is to introduce slow synaptic depression.

3.2 Slow synaptic depression ($\beta > 0$, $\tau_s \gg 1$)

Let us now consider the full neural field model with depressing excitatory connections given by equations (2.1) and (2.2) with $f(u) = H(u - \kappa)$. As in the case $\beta = 0$, there are four possible homogeneous fixed points corresponding to an off-state, a fusion state and two WTA states, and all are stable. Denoting a homogeneous fixed point by (U^*, V^*, Q_u^*, Q_v^*), we have

$$U^* = Q_u^* \overline{w}_e H(U^* - \kappa) - Q_v^* \overline{w}_i H(V^* - \kappa) + I$$
$$Q_u^* = \frac{1}{1 + \beta H(U^* - \kappa)}$$
$$V^* = Q_v^* \overline{w}_e H(V^* - \kappa) - Q_u^* \overline{w}_i H(U^* - \kappa) + I$$
$$Q_v^* = \frac{1}{1 + \beta H(V^* - \kappa)}$$

with $\overline{w}_e, \overline{w}_i$ given by equation (3.6). Hence, the fusion state is now

$$(U^*, V^*) = \left(\frac{\overline{w}_e - \overline{w}_i}{1 + \beta} + I, \frac{\overline{w}_e - \overline{w}_i}{1 + \beta} + I \right),$$
$$(Q_u^*, Q_v^*) = \left(\frac{1}{1 + \beta}, \frac{1}{1 + \beta} \right), \tag{3.15}$$

and occurs when $I > \kappa - (\bar{w}_e - \bar{w}_i)/(1 + \beta)$. This case is more likely for very strong depression (β large), since cross inhibition will be weak, or when the local connections are strong and excitation-dominated. The left eye dominant WTA state now takes the form

$$(U^*, V^*) = \left(\frac{\overline{w}_e}{1 + \beta} + I, I - \frac{\overline{w}_i}{1 + \beta} \right),$$
$$(Q_u^*, Q_v^*) = \left(\frac{1}{1 + \beta}, 1 \right) \tag{3.16}$$

whereas the right eye dominant WTA state becomes

$$(U^*, V^*) = \left(I - \overline{w}_i, \frac{\overline{w}_e}{1 + \beta} + I \right),$$
$$(Q_u^*, Q_v^*) = \left(1, \frac{1}{1 + \beta} \right) \tag{3.17}$$

The WTA states exist provided that

$$I > \kappa - \frac{\overline{w}_e}{1 + \beta}, \quad I < \kappa + \frac{\overline{w}_i}{1 + \beta}$$

This will occur in the presence of weak depression (β small) and strong cross-inhibition such that depression cannot exhaust the dominant hold one population has on the other. Previously, we have shown that equations (2.1) and (2.2) also support homogeneous limit cycle oscillations in which there is periodic switching between left and right eye dominance consistent with binocular rivalry [25]. Since all the fixed points are stable, it follows that such oscillations cannot arise via a standard Hopf bifurcation. Indeed, we find bistable regimes in which a rivalry state coexists with a fusion state as illustrated in Figure 3. (Such behavior persists in the case of smooth sigmoid firing rate functions, at least for sufficiently high gain [25]).

Suppose that the full system given by equations (2.1) and (2.2) is initially in a stable right eye dominated WTA state, and is then perturbed away from this state by introducing a propagating front that generates a switch from right to left eye dominance. We further assume that over a finite spatial domain of interest the time taken for the
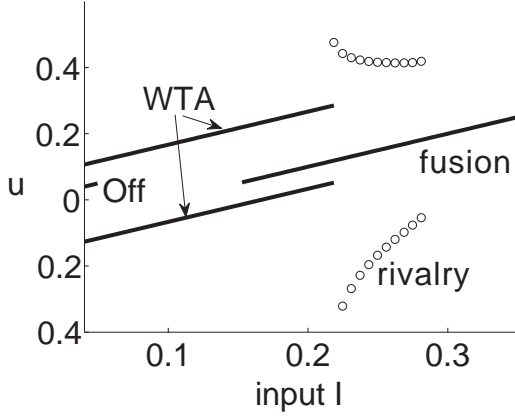
Fig. 3 Bifurcation diagram showing homogeneous solutions for the left population activity u as a function of the input amplitude I. Solid lines represent stable states, whereas circles represent the maximum and minimum of rivalrous oscillations. It can be seen that there are regions of off/WTA bistability, WTA/fusion bistability, and fusion/rivalry bistability. Parameters are $\tau_s = 500$, $\kappa = 0.05$, $\beta = 5$, $\overline{w}_e = 0.4$ and $\overline{w}_i = -1$.

$$u(x,t) = I + Q_u \int_0^\infty \eta(s) G_e[u](x, t-s)ds$$
$$-Q_v \int_0^\infty \eta(s) G_i[v](x, t-s)ds \quad (3.18)$$

$$v(x,t) = I + Q_v \int_0^\infty \eta(s) G_e[v](x, t-s)ds$$
$$-Q_u \int_0^\infty \eta(s) G_i[u](x, t-s)ds. \quad (3.19)$$

with $G_{e,i}$ given by equation (3.5). The analysis of the existence of a traveling wave front solution proceeds along identical lines to section 3.1, except that now the asymptotic states take the form

$$\mathbf{X}_L = (q_u\overline{w}_e + I, I - q_v\overline{w}_i), \; \mathbf{X}_R = (I - q_u\overline{w}_i, q_v\overline{w}_e + I).$$

We thus obtain the following modified threshold conditions:

$$\kappa = \int_0^\infty \eta(s)\Psi_{\xi_0}(cs)ds + I, \quad (3.20)$$

$$\kappa = \int_0^\infty \eta(s)\Phi_{\xi_0}(-cs)ds + I, \quad (3.21)$$

with Ψ and Φ defined by

$$\Psi_{\xi_0}(z) = Q_u \int_z^\infty w_e(y)dy - Q_v \int_{-\infty}^{z-\xi_0} w_i(y)dy. \quad (3.22)$$

$$\Phi_{\xi_0}(z) = Q_v \int_z^\infty w_e(y)dy - Q_u \int_{-\infty}^{z-\xi_0} w_i(y)dy. \quad (3.23)$$

It can be seen that synaptic depression breaks the symmetry of the consistency equations, and this will allow us to find solutions for c, ξ_0 and thus establish the existence of traveling front solutions.

wave front to propagate is much smaller than the relaxation time τ_s of synaptic depression. Thus, to a first approximation we can ignore the dynamics of the depression variables and assume that they are constant, that is, $(q_u(x,t), q_v(x,t)) = (Q_u, Q_v)$ with $Q_u = 1$ and $Q_v = (1 + \beta)^{-1}$. A similar adiabatic approximation can also be made if the network is in a binocular rivalry state, provided that (a) the duration of wave propagation is short compared to the natural switching period and (b) the induction of the wave does not occur close to the point at which spontaneous switching occurs. In this case Q_u and Q_v will not be given by the WTA solution, but we can assume that $Q_u \neq Q_v$. Under the adiabatic approximation, we obtain a slightly modified version of equations (3.1) and (3.2) given by

3.3 Calculation of wave speed

In order to establish the existence of a wave speed c and a threshold crossing point ξ_0, define the functions

$$F_1(c,\xi_0) = \int_0^\infty \eta(s)\Psi_{\xi_0}(cs)ds \qquad (3.24)$$

and

$$F_2(c,\xi_0) = \int_0^\infty \eta(s)\Phi_{\xi_0}(-cs)ds. \qquad (3.25)$$

Evaluating the integrals using equations (2.5), (3.22), (3.23) and $\eta(s) = e^{-s}$ gives (for $c > 0$)

$$\begin{aligned} F_1(c,\xi_0) = &\frac{a_e Q_u}{2}\left(1 - e^{\frac{\sigma_e^2}{2\tau_f^2 c^2}}\mathrm{Erfc}\left[\frac{\sigma_e}{\sqrt{2}\tau_f c}\right]\right)\\ &-\frac{a_i Q_v}{2}\left(\mathrm{Erfc}\left[\frac{\xi_0}{\sqrt{2}\sigma_i}\right]\right.\\ &\left. -e^{\frac{\sigma_i^2 - 2\tau_f c\xi_0}{2\tau_f^2 c^2}}\mathrm{Erfc}\left[\frac{\sigma_i^2 - \tau_f c\xi_0}{\sqrt{2}\sigma_i\tau_f c}\right]\right) \end{aligned} \qquad (3.26)$$

$$\begin{aligned} F_2(c,\xi_0) = &\frac{a_e Q_v}{2}\left(1 + e^{\frac{\sigma_e^2}{2\tau_f^2 c^2}}\mathrm{Erfc}\left[\frac{\sigma_e}{\sqrt{2}\tau_f c}\right]\right)\\ &-\frac{a_i Q_u}{2}\left(\mathrm{Erfc}\left[\frac{\xi_0}{\sqrt{2}\sigma_i}\right]\right.\\ &\left. -e^{\frac{\sigma_i^2 + 2\xi_0\tau_f c}{2\tau_f^2 c^2}}\mathrm{Erfc}\left[\frac{\sigma_i^2 + \xi_0\tau_f c}{\sqrt{2}\sigma_i\tau_f c}\right]\right) \end{aligned} \qquad (3.27)$$

where

$$\mathrm{Erfc}(x) = \frac{2}{\sqrt{\pi}}\int_x^\infty e^{-t^2}dt$$

is the complementary error function. Subtracting equation (3.21) from (3.20), we then have the implicit equation

$$G(c,\xi_0) \equiv F_1(c,\xi_0) - F_2(c,\xi_0) = 0. \qquad (3.28)$$

It is straightforward to show that for fixed ξ_0,

$$\lim_{c\to\infty} G(c,\xi_0) > 0, \quad \lim_{c\to-\infty} G(c,\xi_0) < 0.$$

Hence, the intermediate value theorem guarantees at least one solution $c = c(\xi_0)$, which is differentiable by the implicit function theorem. If $Q_u =$

Q_v, then $F_1(0,\xi_0) = F_2(0,\xi_0)$ and the only point where G vanishes is at $c = 0$. On the other hand, if $Q_v \neq Q_u$ then $G(0,\xi_0) \neq 0$ for all finite ξ_0 so that $c(\xi_0) \neq 0$. Given a solution $c = c(\xi_0)$ of equation (3.28), the existence of a traveling wavefront solution reduces to the single threshold condition

$$\kappa = F_1(c(\xi_0),\xi_0) + I. \qquad (3.29)$$

We find that there exists a unique traveling front solution for a range of values of κ.

In Figs. 4 and 5, we plot wave speed as a function of various model parameters. We choose baseline parameter values such that spontaneous oscillations and traveling fronts co-exist, as found experimentally [22, 23]. The model wave speed is of the order $c = 1$ in dimensionless units, that is, $c = \sigma_e/2\tau$ where σ_e is the range of excitation and τ is the membrane time constant. In the psychophysical experiments of Kang *et. al.* [22, 23], it was found that binocular rivalry waves took approximately 0.8 seconds to traverse 2 degrees of the visual field. The magnification factor in humans throughout the foveal region is approximately $0.4cm/deg$, which corresponds to $0.8cm$ of cortex. Hence the wave speed we would expect to see in cortex based on the psychophysical experiments is approximately $10mm/sec$. This is consistent with our analytical results, if we take σ_e to be of the order $200\mu m$ and τ to be of the order 10 msec. Fig. 4 shows that increasing the strength of excitation (cross–inhibition) increases (decreases) the speed of the wave, whereas Fig. 5(a) shows that the speed of the wave decreases as the threshold κ increases. However, these parameters cannot be manipulated in psychophysical experiments. On the other hand, it is possible to vary the contrast of the sinusoidal grating stimuli. For example, Kang *et. al.*[22, 23] showed that increasing the stimulus contrast increases wave speed. This is consistent with Fig. 5(b), which plots wave speed as a function of in-
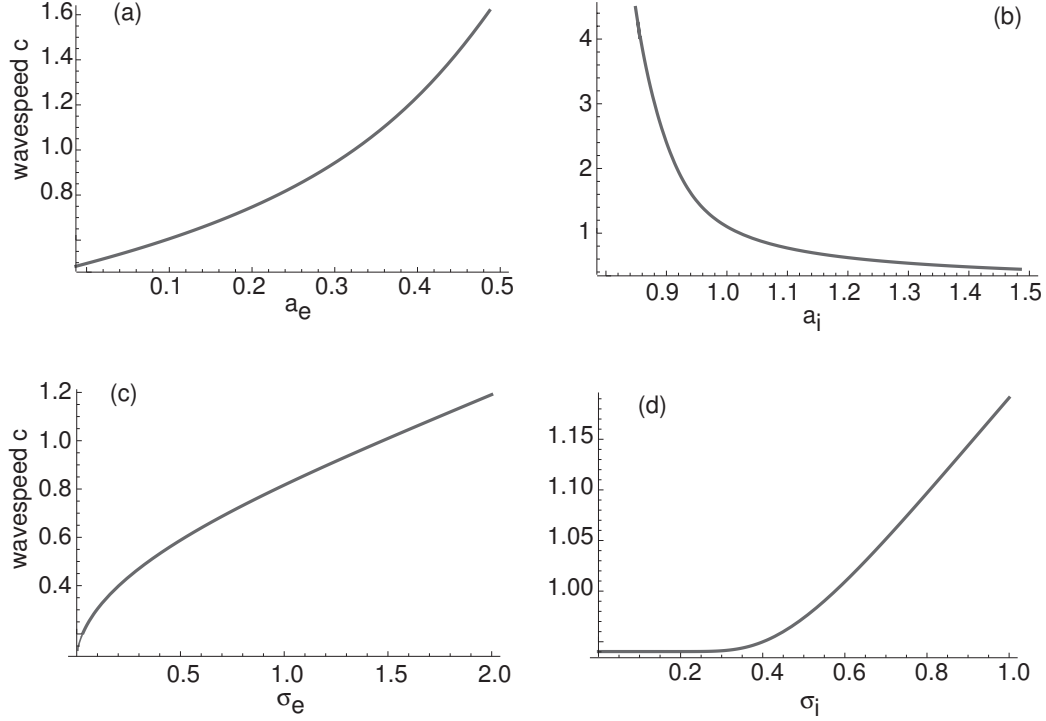
Fig. 4 Plot of wave speed c as a function of various weight parameters: (a,b) the amplitudes a_e, a_i and (c,d) the length constants σ_e, σ_i. The default parameters are taken to be $a_i = 1, a_e = 0.4, \sigma_i = 1, \sigma_e = 2, \beta = 5, \kappa = 0.05, I = 0.24, Q_u = 0.42, Q_v = 0.25$ and the corresponding wave speed is $c = 1.2$. For this set of parameters, the network operates in a regime that supports both traveling waves and homogeneous oscillatory solutions, that is, spontaneous switching occurs in the absence of traveling waves.

put amplitude I. Another variable that could be manipulated is the time at which a rivalry wave is induced relative to the phase of the limit cycle representing spontaneous rivalry oscillations. In our model, under the adiabatic approximation, this would correspond to changing the values of Q_u and Q_v. In Fig. 5(c) we plot wave speed as a function of $\Delta Q = (Q_u - Q_v)/2$ with $Q_u + Q_v$ fixed. It can be seen that c increases with ΔQ, which is analogous to inducing a wave closer to the point at which spontaneous switching would occur (see also section IV). Note that in the experimental protocol of Kang *et al* [22, 23], see Fig. 1, the wave speed is determined after averaging with respect to the switching events induced by a sequence of periodic trigger stimuli rather than a single trig-

gering event. In terms of our model, this would correspond to averaging the wave speed with respect to a range of values of Q_u and Q_v, since spontaneous binocular rivalry oscillations are actually noisy. Hence, the dependence of wave speed on the timing of the inducing stimuli relative to the phase of spontaneous oscillations is effectively reduced. However, Kang *et al* did find that there is an optimal trigger period for inducing reliable switching that depends on the natural period of spontaneous oscillations. It is likely that this phase–locking phenomenon reflects some residual dependence of wave propagation on the relative timing of the trigger stimuli. Finally, a typical example of a wavefront profile is shown in Fig. 5(d). Note that the symmetry breaking mechanism necessary
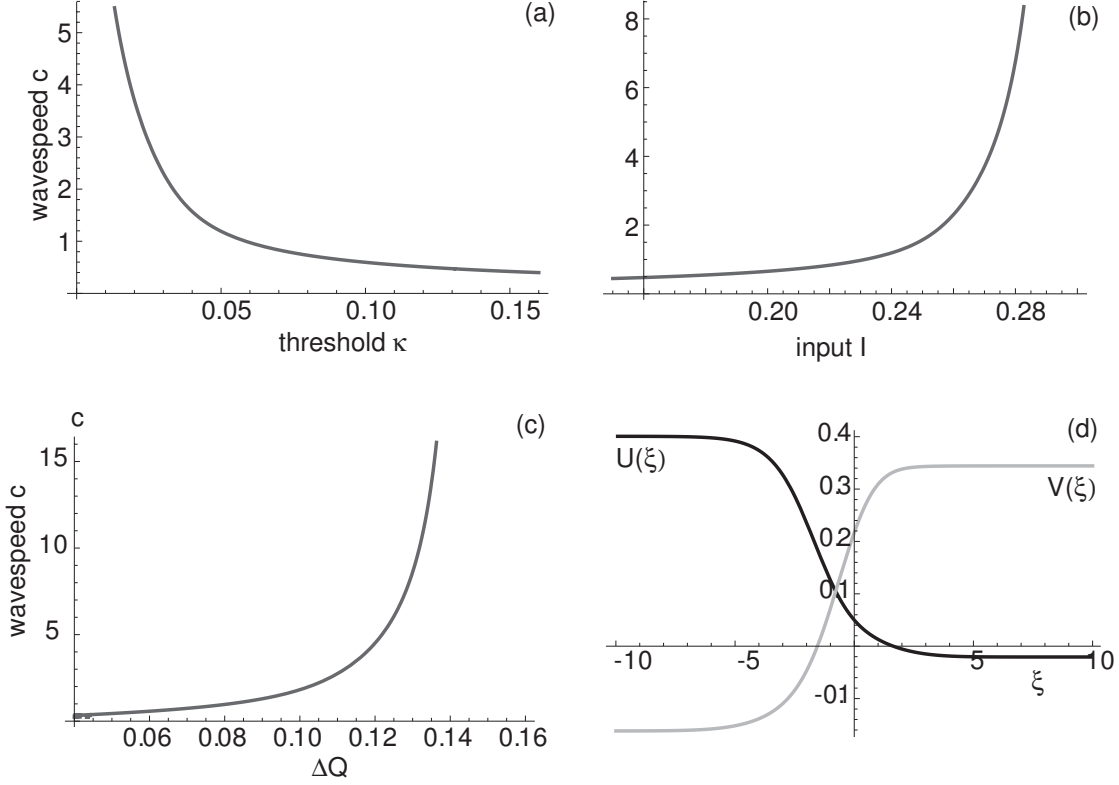
Fig. 5 (a-c) Plot of wave speed c as a function of (a) the threshold κ, (b) the external input strength I and (c) ΔQ where $Q_u = Q_0 + \Delta Q, Q_v = Q_0 - \Delta Q$ with $Q_0 = 0.335$. (d) Plot of right–moving traveling front solution in which in which a high activity state invades the suppressed left eye network whilst retreating from the dominant right eye network. Parameters are at the baseline values of Fig. 4 unless specified otherwise.

to support wave propagation is reflected by the fact that $\lim_{\xi \to -\infty} U(\xi) > \lim_{\xi \to \infty} V(\xi)$. That is, the initial activity in the dominant right eye is depressed compared to the final activity in the dominant left eye (under the adiabatic approximation).

3.4 Wave stability

In order to determine wave stability, we linearize equations (3.18) and (3.19) around the traveling wave solution $(U(\xi), V(\xi))$ with Q_u, Q_v fixed. Writing $u(x, t) = U(\xi) + r(\xi)e^{\lambda t}$ and $v(x, t) = V(\xi) + p(\xi)e^{\lambda t}$ with $\text{Re}[\lambda] > -1$, we obtain the linear system

$$
\begin{aligned}
r(\xi) = Q_u \int_0^\infty \eta(s) \int_{-\infty}^\infty w_e(y) r(\xi + cs - y) e^{-\lambda s} \\
\times \delta(U(\xi + cs - y) - \kappa) dy ds \\
- Q_v \int_0^\infty \eta(s) \int_{-\infty}^\infty w_i(y) p(\xi + cs - y) e^{-\lambda s} \\
\times \delta(V(\xi + cs - y) - \kappa) dy ds
\end{aligned}
$$

$$
\begin{aligned}
p(\xi) = Q_v \int_0^\infty \eta(s) \int_{-\infty}^\infty w_e(y) p(\xi + cs - y) e^{-\lambda s} \\
\times \delta(V(\xi + cs - y) - \kappa) dy ds \\
- Q_u \int_0^\infty \eta(s) \int_{-\infty}^\infty w_i(y) r(\xi + cs - y) e^{-\lambda s} \\
\times \delta(U(\xi + cs - y) - \kappa) dy ds,
\end{aligned}
$$

where $\delta(U - \kappa)$ denotes the Dirac delta function. Using the threshold conditions $U(0) = \kappa$, $V(\xi_0) =$

κ and a property of Dirac delta functions, we have

$$\delta(U(\xi)) = \frac{\delta(\xi)}{|U'(0)|}, \quad \delta(V(\xi)) = \frac{\delta(\xi - \xi_0)}{|V'(\xi_0)|} \quad (3.30)$$

Hence,

$$r(\xi) = Q_u \int_0^\infty \eta(s) w_e(\xi + cs) \frac{r(0)}{|U'(0)|} e^{-\lambda s} ds$$
$$- Q_v \int_0^\infty \eta(s) w_i(\xi + cs - \xi_0) \frac{p(\xi_0)}{|V'(\xi_0)|} e^{-\lambda s} ds \quad (3.31)$$

$$p(\xi) = Q_v \int_0^\infty \eta(s) w_e(\xi + cs - \xi_0) \frac{p(\xi_0)}{|V'(\xi_0)|} e^{-\lambda s} ds$$
$$- Q_u \int_0^\infty \eta(s) w_i(\xi + cs) \frac{r(0)}{|U'(0)|} e^{-\lambda s} ds. \quad (3.32)$$

Introducing an appropriate norm on the space of functions $(r(\xi), p(\xi))$, the linear equations (3.31) and (3.32) generate a well defined spectral problem. In particular, the discrete spectrum of eigenvalues λ is obtained by finding solutions $r(\xi)$ and $p(\xi)$ that decay sufficiently fast as $|\xi| \to \infty$ – the rate of decay is determined by the weight functions w_e, w_i. These eigensolutions can be found by setting $\xi = 0$ in equation (3.31) and $\xi = \xi_0$ in equation (3.32), and solving the resulting self–consistency equations for $r(0)$ and $p(\xi_0)$:

$$\begin{pmatrix} r(0) \\ p(\xi_0) \end{pmatrix} = \begin{pmatrix} \frac{Q_u \widehat{W}_e(\lambda, 0)}{|U'(0)|} & -\frac{Q_v \widehat{W}_i(\lambda, -\xi_0)}{|V'(\xi_0)|} \\ -\frac{Q_u \widehat{W}_i(\lambda, \xi_0)}{|U'(0)|} & \frac{Q_v \widehat{W}_e(\lambda, 0)}{|V'(\xi_0)|} \end{pmatrix} \begin{pmatrix} r(0) \\ p(\xi_0) \end{pmatrix}$$

where

$$\widehat{W}_p(\lambda, \xi) = \int_0^\infty \eta(s) w_p(cs + \xi) e^{-\lambda s} ds$$

for $p = e, i$. The self–consistency equation has a non-trivial solution provided that λ is a zero of the function

$$E(\lambda) = \det \begin{pmatrix} \frac{Q_u \widehat{W}_e(\lambda, 0)}{|U'(0)|} - 1 & -\frac{Q_v \widehat{W}_i(\lambda, -\xi_0)}{|V'(\xi_0)|} \\ -\frac{Q_u \widehat{W}_i(\lambda, \xi_0)}{|U'(0)|} & \frac{Q_v \widehat{W}_e(\lambda, 0)}{|V'(\xi_0)|} - 1 \end{pmatrix}$$

We identify $E(\lambda)$ with the so–called Evans function of the traveling wave solution [42, 13, 31].

That is, the complex number λ is an eigenvalue of the linear system if and only if $E(\lambda) = 0$. Moreover, the algebraic multiplicity of each eigenvalue is equal to the order of the corresponding zero of the Evans function. It can be shown that $E(\lambda)$ is analytic in λ and thus normal numeric root finding may be used to find λ. The wave will be linearly stable if all non-zero eigenvalues λ have negative real part and $\lambda = 0$ is a simple eigenvalue. The existence of a zero eigenvalue reflects translation invariance of the dynamical system given by equations (3.18) and (3.19). (Note that there is also a continuous part of the spectrum, but this always lies in the left–half complex λ–plane and thus does not contribute to any wave instabilities [13, 31]). Numerically plotting the zero sets $\mathrm{Re}[E[\lambda]]$ and $\mathrm{Im}[E[\lambda]]$ for the baseline parameter values, we find that there exists only a single eigenvalue (at $\lambda = 0$), indicating that the traveling front is linearly stable. This result persists for other choices of parameters for which a traveling front exists.

4 Numerical simulations

In our analysis of binocular rivalry waves (section 3), we neglected the dynamics of the depression variables by making an adiabatic approximation. In this section we numerically solve the full system of equations (2.1) and (2.2) and show that traveling fronts persist when the dynamics of the depression variables is included.

We begin by considering a single trigger stimulus in the form of a temporary, spatially localized increase in the input strength to the suppressed eye network, which for concreteness we take to be the left eye. Thus,

$$I_u(x, t) = \Theta(t - t_0)\Theta(\Delta t + t_0 - t)\Theta(\Delta x - |x|)\Delta I$$
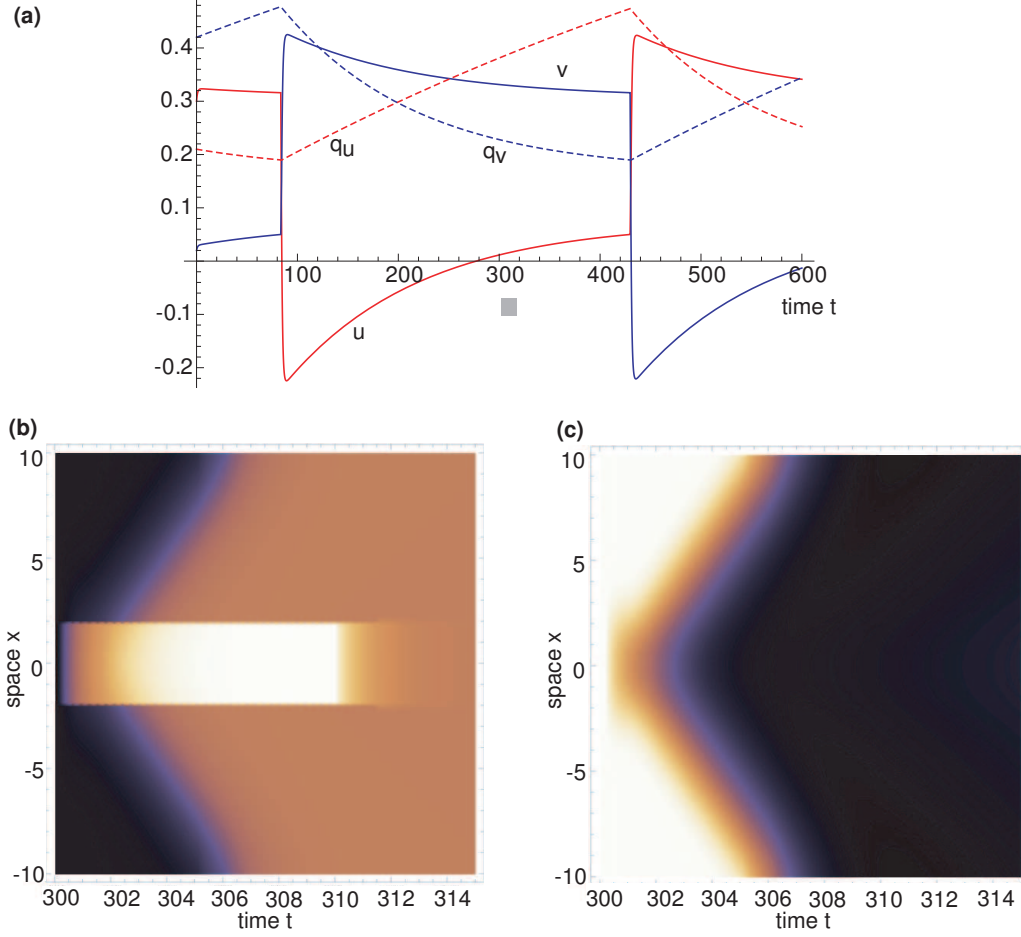$$+ I,$$
$$I_v(x, t) = I$$

Fig. 6 Induction of a solitary binocular rivalry wave. Parameter values are $\tau_s = 800, a_i = 1, a_e = 0.4, \sigma_i = 1, \sigma_e = 2, \beta = 5, \kappa = 0.05, I = 0.24$. (a) Homogeneous oscillatory solution in which there is spontaneous periodic switching between left and right eye dominance. Plot against time of the left eye neural activity u (solid red), the right eye neural activity v (solid blue) together with the corresponding depression variables q_u (dashed red) and q_v (dashed blue). (b,c) Space–time plots of $u(x,t)$ and $v(x,t)$ following onset of the trigger stimulus to the left eye at time $t_0 = 300$, which involves a temporary increase in the input strength I_u from 0.24 to 0.74 within the domain $-2 \leq x \leq 2$. (The duration of the trigger stimulus is also indicated by the grey bar in part (a)). Lighter (darker) colors indicate higher (lower) activity values. The mean wave speed of the front (calculated numerically)) is $c \sim 2$. This is in good agreement with our analytical results based on taking fixed depression variables $Q_u = q_u(t_0), Q_v = q_v(t_0)$.

where Θ is the Heaviside function. The trigger stimulus is switched on at $t = t_0$ and switched off at time $t = t_0 + \Delta t$, and consists of an increase in input strength ΔI in a region of width $2\Delta x$ centered about $x = 0$. In order for traveling waves to be induced in our model, the size Δx of the excited region has to be of the order of σ_e, otherwise the

effects of the perturbation simply die away. This is consistent with the size of perturbation used in the experiments by Kang *et. al.* [22, 23], which was of size 0.2 degrees, corresponding to 0.8mm of cortical tissue. Their perturbations were shown for 200ms, similar to the time interval of $\Delta t = 10$ used in our simulations. Two examples of induced binocu-
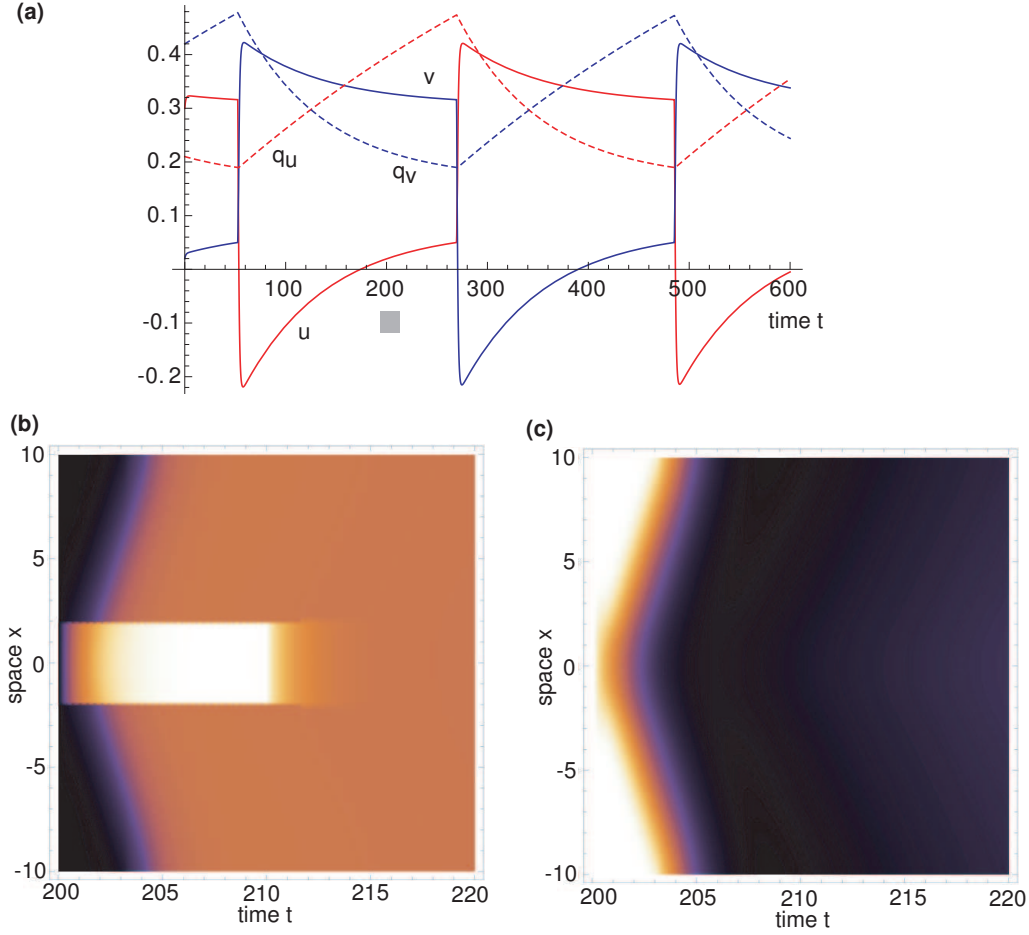
(a)

(b)

(c)

Fig. 7 Same as Fig. 6 except that $\tau_s = 500$. Onset of trigger stimulus is at $t_0 = 200$. Both the frequency of spontaneous oscillations and the speed of the wave are higher with $c \sim 3$

lar rivalry waves are shown in Fig. 6 and Fig. 7. In these examples, the wave speed is fast relative to the frequency of spontaneous oscillations so the depression variables change very little over the time during which the wave is traveling. Hence, there is a good match between properties of the numerically simulated wave and our analytical results of section 3. In Fig. 8 we further illustrate the good agreement between theory and numerics by plotting the location x vs. time t of a fixed point in traveling wave coordinates given by $u(x, t) = 0.3$. As expected, there is a small variation in wave

speed due to the dynamics of the depression variables but the mean speed is consistent with theory.

Since the network operates in a regime where spontaneous rivalry oscillations occur in the absence of any trigger stimuli, it follows from our analytical results (section 3) that the speed of the induced wave will depend on which phase of the limit cycle the trigger stimulus is initiated. That is, let the time of stimulus onset be $t_0 = nT + \theta T/(2\pi)$, where T is the period of spontaneous oscillations, n is an integer and $0 \leq \theta < 2\pi$. Denoting the oscillatory solution of the depression variables on the limit cycle by $\{q_u^*(\phi), q_v^*(\phi)|0 \leq \phi < 2\pi\}$, we set
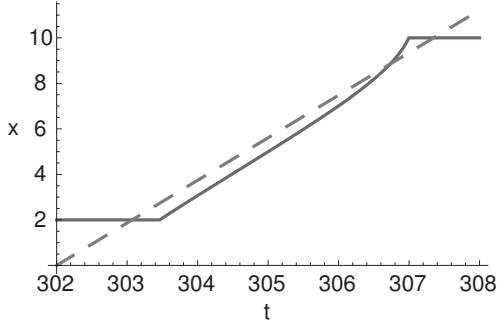
Fig. 8 Plot of the spatial location x vs. time t of the point at which $u(x,t) = 0.3$ (solid curve). Same parameter values as Fig. 6 with onset of trigger stimulus at $t_0 = 300$. There is a latency period before the wave front reaches the initial location of the point $u = 0.3$. The wave front moves with approximately constant speed that is consistent with the theoretical value as indicated by the dashed line of constant slope.
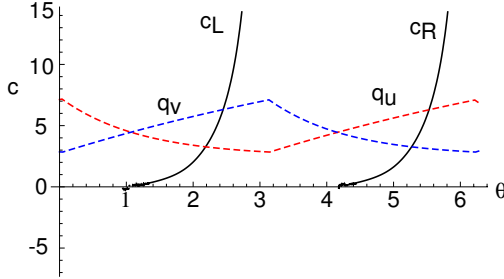

Fig. 9 Wavespeed vs phase (solid curve) along one cycle of spontaneous oscillations. Here c_L (c_R) denotes the speed of a wave induced in the suppressed left (right) eye network. Also shown are the temporal profiles of the depression variables (dashed curves). Same parameter values as Fig. 7.

$Q_u = q_u^*(\theta), Q_v = q_v^*(\theta)$ where Q_u, Q_v are the fixed values appearing in equations (3.18) and (3.19) under the adiabatic approximation. It follows that the wave speed calculated from equation (3.29) is phase–dependent: $c = c(Q_u, Q_v) = c(\theta)$. An example plot of wave speed vs phase θ is shown in Fig. 9. We see that a rivalry wave only exists if the trigger stimulus occurs in the latter $\sim \frac{2}{3}$ of the half–cycle, with faster waves induced closer to the point of spontaneous switching. Now suppose that we keep the phase of the trigger stimulus fixed and

determine how both the natural frequency $1/T$ and wave speed c vary with stimulus contrast I. The results are presented in Fig. 10. The wave speed is determined from equation (3.29), whereas the period T is calculated using the analytical results of [25]. It can be seen that faster natural alternation rates lead to faster wave speeds. (Wavespeed and frequency also covary with changes in the depression rate constant β, for example). Interestingly, an analogous result was obtained by Kang *et. al.* [22, 23], who found experimentally that traveling waves were faster for subjects whose natural rate of binocular rivalry oscillations was higher. However, as noted in section 3, the wave speed was averaged over several cycles of trigger stimuli in the psychophysical experiments. Given the stochastic nature of spontaneous oscillations, we expect such averaging to reduce the dependence on the phase θ.

In order to relate our model more closely with the experimental protocol of Kang *et al.* [22, 23], we have also carried out simulations of the full model (2.1) and (2.2) in the presence of additive noise and periodic trigger stimuli. For the sake of illustration, we introduce spatially uncorrelated additive white noise terms to the the dynamical equations for the depression variables according to

$$\tau_s \frac{\partial q_u(x,t)}{\partial t} = 1 - q_u(x,t) - \beta q_u(x,t) f(u(x,t))$$
$$+ \sigma \xi_u(x,t) \qquad (4.1)$$
$$\tau_s \frac{\partial q_v(x,t)}{\partial t} = 1 - q_v(x,t) - \beta q_v(x,t) f(v(x,t))$$
$$+ \sigma \xi_v(x,t) \qquad (4.2)$$

with

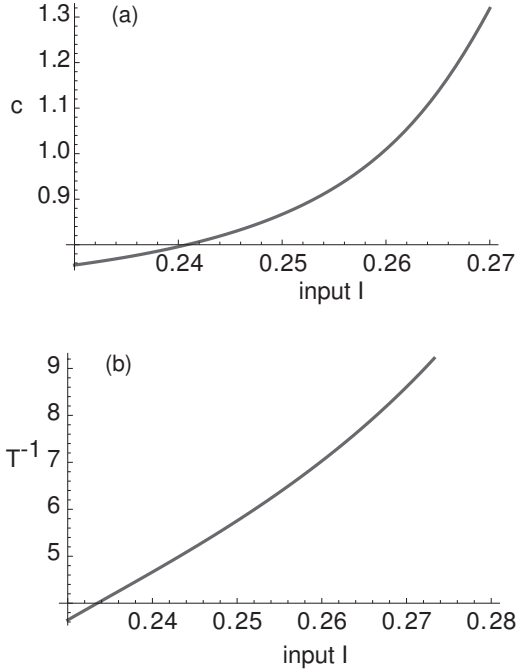$$\langle \xi_u(x,t) \rangle = \langle \xi_v(x,t) \rangle = 0$$

Fig. 10 Wavespeed and frequency of spontaneous oscillations covary. Plot of (a) wavespeed c and alternation rate $\frac{1}{T}$ as a function of stimulus contrast I. The depression parameters Q_u, Q_v are determined by taking the phase θ of stimulus onset to be $\theta = 3\pi/2$. All other parameters are given by the baseline values of Fig. 4.

and

$$\langle \xi_u(x,t)\xi_u(x',t') \rangle = \delta(x - x')\delta(t - t'),$$
$$\langle \xi_v(x,t)\xi_v(x',t') \rangle = \delta(x - x')\delta(t - t')$$
$$\langle \xi_u(x,t)\xi_v(x',t') \rangle = 0.$$

Furthermore, the inputs I_u and I_v in equations (2.1a) and (2.2a) take the form

$$I_u(x,t) = I + \sum_{m=0,2,4,\ldots} \Theta(t - t_0 - mT_0)$$
$$\times \Theta(\Delta t + t_0 + mT_0 - t)\Theta(\Delta x - |x|)\Delta I,$$
$$I_v(x,t) = I + \sum_{m=1,3,5,\ldots} \Theta(t - t_0 - mT_0)$$
$$\times \Theta(\Delta t + t_0 + mT_0 - t)\Theta(\Delta x - |x|)\Delta I$$

That is, starting at time $t = t_0$, the left and right eye networks receive a T_0–periodic alternating sequence of trigger stimuli, each of which consists of
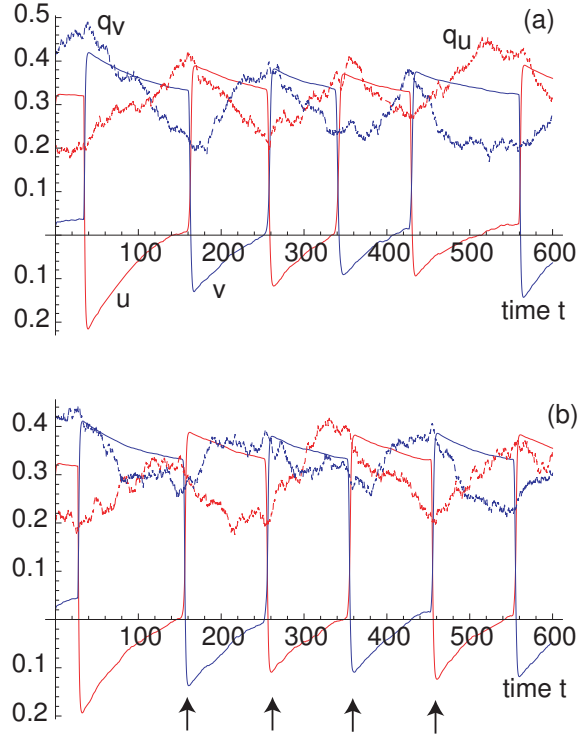

Fig. 11 Comparison of spontaneous and periodically forced binocular rivalry oscillations in the presence of noise. The time evolution of the activity and depression variables are shown at a fixed spatial location ($x = 7$). Noise strength $\sigma = 1$ and all other parameter values are as in Fig. 7. Left (right) eye variables are shown in red (blue) with noise in the depression variables. (a) Homogeneous oscillatory solution, which shows some irregularity due to noise in the depression variables (b) Periodically triggered alternations in dominance. Onset of each trigger stimulus is indicated by an arrow. Initial trigger occurs at $t_0 = 150$ and time between triggers is $T_0 = 100$.

an enhancement of input strength in the domain $|x| < \Delta x$ that has duration Δt.

Results from numerical simulations of the full model given by equations (2.1a), (2.2a), (4.1) and (4.2) are shown in Figs. 11 and 12. It can be seen that provided the noise strength σ is not too large then there is reliable switching between left and right eye dominance that phase locks to the periodic trigger stimuli. However, as σ increases to a value of around $\sigma \approx 2$, phase locking starts to
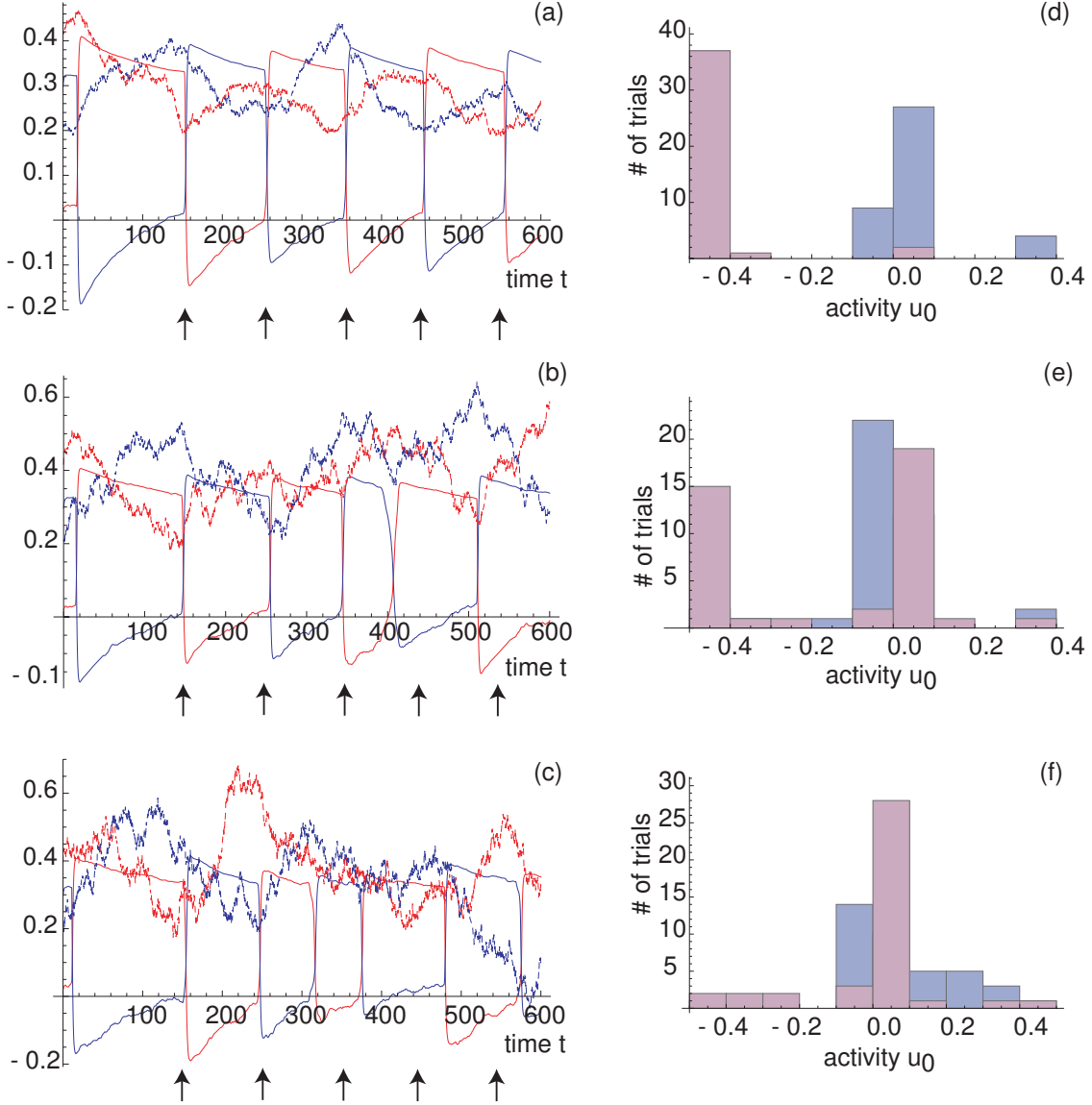
Fig. 12 Breakdown of mode–locking as noise strength increases. (a-c). The time evolution of the activity and depression variables are shown at a fixed spatial location ($x = 7$) for various noise strengths: (a) $\sigma = 1$, (b) $\sigma = 2$, (c) $\sigma = 3$. All other parameter values are as in Fig. 11. Onset of each trigger stimulus is indicated by an arrow. Initial trigger occurs at $t_0 = 150$ and time between triggers is $T_0 = 100$. (d-e) Corresponding histograms showing how the change in activity $\Delta u = u(x, t_1) - u(x, t_2)$ at a fixed location $x = 7$ and two different times ($t_1 = 450, t_2 = 470$) is distributed over multiple trials. Pink (purple) bars indicate distribution in the presence (absence) of periodic trigger stimuli
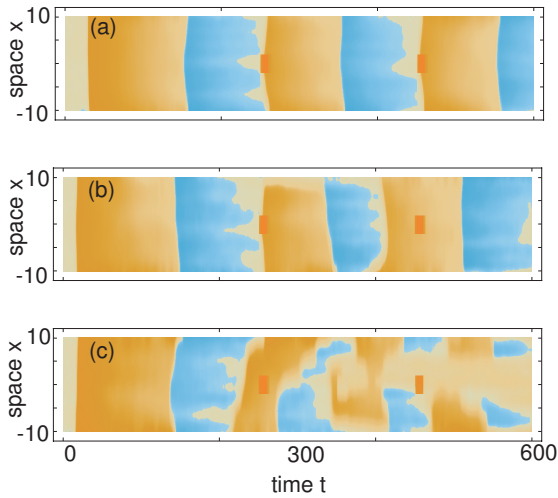
Fig. 13 Space–time plots of periodically triggered binocular rivalry waves in left eye network for increasing levels of noise: (a) $\sigma = 1$, (b) $\sigma = 2$, (c) $\sigma = 3$. Red rectangles indicate duration and spatial extent of trigger stimuli. All other parameters as in Fig. 12.

break down. As a further illustration of how mode–locking depends on the level of noise, we also plot in Fig. 12 histograms comparing the spontaneous and forced distributions of activity $\Delta u = u(x, t_1) - u(x, t_2$ at a fixed location x and fixed times time t_1, t_2 over multiple trials (simulation runs). For a noise strength $\sigma = 1$ it can be seen that mode locking causes a very strong tendency to be in the completely opposite state to that without mode locking, whereas for higher noise strengths $\sigma = 2, 3$ the distribution is much wider and in some situations the forcing did not change the state from the unforced case (breakdown of mode-locking). Finally, the disruption of binocular rivalry waves with increasing noise is illustrated by the space–time plots of the left network activity variable $u(x, t)$ in Fig. 13.

So far we have taken the firing rate function to be the Heaviside function (2.4) in order to compare our numerics with the analysis of section 3. As in many previous studies of neural field equations

dating back to Amari [2], the use of Heavisides allowed us to construct explicit traveling wave solutions and to derive an explicit formula for the speed of the wave. However, it is important to check that the same basic mechanism of wave induction and propagation carries over to more realistic sigmoidal rate functions. This is indeed found to be the case, as is illustrated in Fig. 14. The speed of the wave is more variable than the Heavside case but is still comparable in magnitude to theoretical predictions.

Note on simulations. All deterministic simulations were carried out by discretizing space and solving the resulting system of ODEs with Mathematica 8.0's ODE solver (NDSolve). Discretization of the neural field model with additive noise generated a system of stochastic ODEs, which were then simulated in C++ code (with boost and Intel TBB) using the Euler–Maruyama method.

5 Discussion

In this paper we analyzed a neural field model of binocular rivalry waves in primary visual cortex. Formulating the problem in terms of continuum neural field equations allowed us to study the short time behavior associated with the propagation of eye dominance from an analytical perspective. In particular, we established that in order for traveling waves to exist, a symmetry breaking mechanism needs to be present. That is, the equations for the left and right eye networks have to be different on the time scales during which traveling waves propagate. We identified one possible mechanism for providing the necessary symmetry breaking, namely, synaptic depression. However any form of slow adaptation would work including spike frequency adaptation. We then showed analytically that for plausible values of biological
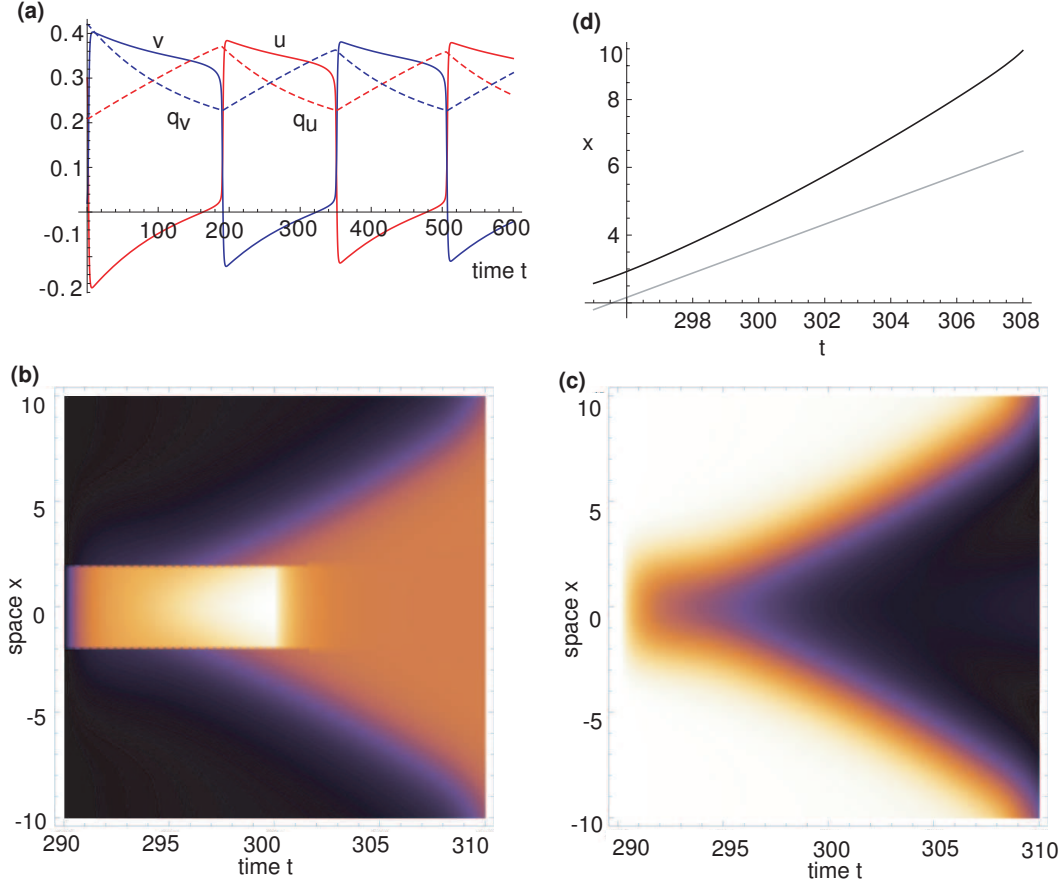
Fig. 14 Induction of a solitary binocular rivalry wave in the case of a smooth sigmoidal firing rate function. Gain of sigmoid is $\eta = 80$. Other parameter values are as in Fig. 6 . (a) Homogeneous oscillatory solution in which there is spontaneous periodic switching between left and right eye dominance. Plot against time of the left eye neural activity u (solid red), the right eye neural activity v (solid blue) together with the corresponding depression variables q_u (dashed red) and q_v (dashed blue). (b,c) Space–time plots of $u(x,t)$ and $v(x,t)$ following onset of the trigger stimulus to the left eye at time $t_0 = 290$, which involves a temporary increase in the input strength I_u from 0.24 to 0.74 within the domain $-2 \le x \le 2$. Lighter (darker) colors indicate higher (lower) activity values. (d) Plot of the spatial location x vs. time t of the point at which $u(x,t) = 0.2$ (black curve). The speed calculated for the Heaviside case is given by the slope of the straight line (grey curve).

parameters such as the range of synaptic interactions and the membrane time constant, we could recover wave speeds similar to those seen in experiments [41, 22, 23]. Moreover, our model exhibited the expected dependence of wave speed on parameters that can be experimentally varied, such as stimulus contrast. It also replicated the experimental finding that wave speed covaries with the natural frequency of spontaneous rivalry oscillations.

Finally, numerical simulations of the full system were in good agreement with our analytical short time scale results in the case of a Heaviside firing rate function. We also found that binocular rivalry waves persisted in the case of smooth sigmoid firing rate functions and in the presence of additive white noise in the depression variable dynamics. However, mode–locking to periodic trigger stimuli

broke down when the noise strength became too large.

In future work it would be interesting to extend our neural field model to a more realistic network topology. Instead of considering one line of neurons for each eye, we could consider a circle of neurons for each point in the visual field - this would allow us to take orientation information into account using an extension of the coupled ring model [10, 11]. We could then investigate the experimental observation that the speed of binocular rivalry waves depends on the orientation of the left and right eye grating stimuli [41]. Another important issue that we only partially addressed in this paper is the role of noise. A number of recent studies have considered stochastic models of binocular rivalry and the statistics of dominance times, but have neglected spatial effects [29, 33, 9]. Developing a better understanding of the combined effects of noise and wave propagation on periodically triggered switching would allow us to address relevant issues such as determining the stimulus trigger period in a noisy system that gives the highest probability of a dominance switch. Such results would add to those already found in this paper (such as wave speed variation with phase angle) that could be experimentally tested and lead to further refinements of the neural field model.

References

1. Abbott, L. F., Varela, J. A., Sen, K. & Nelson, S. B. (1997). Synaptic depression and cortical gain control., *Science*, *275*, 220–224.

2. Amari, S. (1977). Dynamics of pattern formation in lateral-inhibition type neural fields., *Biol Cybern., 27* , 77–87.

3. Angelucci, A., Levitt, J. B., Walton, E. J. S., Hupe, J.-M. , Bullier, J. & Lund, J. S. (2002). Circuits for local and global signal integration in primary visual cortex, *J Neurosci, 22*, 8633–46.

4. Bart, E., Bao, S., & and Holcman, D. (2005). Modeling the spontaneous activity of the auditory cortex., *J Comput Neurosci, 19*, 357–378.

5. Ben-Yishai, R., Bar-Or, R. L. & Sompolinsky, H., (1995). Theory of orientation tuning in visual cortex, *Proc. Natl. Acad. Sci. USA, 92*, 3844–3848.

6. Blake, R. (2001). A primer on binocular rivalry, including current controversies, *Brain and Mind, 2*, 5–38.

7. Blake, R. & Logothetis, N. (2002). Visual competition, *Nature Reviews Neuroscience 3*, 1–11.

8. Blasdel, G. G. (1992). Orientation selectivity, preference, and continuity in monkey striate cortex, *J Neurosci, 12*, 3139–61.

9. Braun, J. C. and Mattia, M. (2010). Attractors and noise: Twin drivers of decisions and multistability. *Neuroimage 52* 740-751.

10. Bressloff, P. C., Cowan, J. D., Golubitsky, M., Thomas, P. J. & Wiener, M. (2001). Geometric visual hallucinations, Euclidean symmetry and the functional architecture of striate cortex, *Phil. Trans. Roy. Soc. B 40*, 299-330.

11. Bressloff, P. C. & Cowan, J. D., (2002). An amplitude equation approach to contextual effects in visual cortex, *Neural Comput, 14*, 493–525.

12. Chance, F. S., Nelson, S. B. & Abbott, L. F. (1998). Synaptic depression and the temporal response characteristics of V1 cells, J Neurosci, 18, 4785–99.

13. Coombes, S. & Owen, M. R. (2004) Evans functions for integral neural field equations with Heaviside firing rate function, *SIAM J. Appl. Dyn. Syst., 3*, 574–600.

14. De Weerd, P., Desimone, R. & Ungerleider, L. G. (1998). Perceptual filling in: a parametric study, *Vision Research, 38*, 2721-2734.

15. Ferster, D. & and Miller, K. D. (2000). Neural mechanisms of orientation selectivity in the visual cortex, *Annu Rev Neurosci, 23*, 441–71.

16. Fox, R. & Rasche, F. (1969). Binocular rivalry and reciprocal inhibition, *Percept. Psychophys., 5*, 215–217.

17. Gold, 1969) & Shubel, E. (2006). The spatiotemporal properties of visual completion measured by response classification. *J. Vision 6*, 356–365.

18. Hadjikhani, N., Sanchez Del Rio, M., Wu, O, Schwartz, D., Bakker, D., et al. (2001). Mechanisms of migraine aura revealed by functional MRI in human visual cortex. *Proc Natl Acad Sci USA, 98*, 4687–4692

19. Hubel, D. H. & Wiesel, T. N. (1962). Receptive fields, binocular interaction and functional architecture in the cat's visual cortex, *J Physiol, 160*, 106–54.

20. Hubel, D. H. & Wiesel, T. N. (1977). Functional architecture of macaque monkey visual cortex, *Proc R Soc Lond B Biol Sci, 198*, 1–59.

21. Jancke, D., Chavane, F., Maaman, S. & Grinvald, A. (2004). Imaging cortical correlates of illusion in early visual cortex. *Nature, 428*, 423-426.

22. Kang, M., Heeger, D. J. & Blake, R. (2009). Periodic perturbations producing phase-locked fluctuations in visual perception. *J. Vision, 9*, 1–12.

23. Kang, M., Heeger, D. J. & Blake, R. (2011). Modulation of spatiotemporal dynamics of binocular rivalry by collinear facilitation and pattern-dependent adaptation. *J. Vision.*

24. Katz, L. C., Gilbert, C. D. & Wiesel, T. N. (1989). Local circuits and ocular dominance columns in monkey striate cortex, *J Neurosci, 9*, 1389–99.

25. Kilpatrick, Z. P. & Bressloff, P. C. (2010). Binocular rivalry in a competitive neural network with synaptic depression. *SIAM J. Appl. Dyn. Syst. 9*, 1303-1347.

26. Laing, C. R. & Chow, C. C. (2002). A spiking neuron model for binocular rivalry, *J Comput Neurosci, 12*, 39–53.

27. Lee, S. -H., Blake, R. & and Heeger, D. J. (2005). Traveling waves of activity in primary visual cortex during binocular rivalry, *Nat Neurosci, 8*, 22–23.

28. Loxley, P. N. & Robinson, P. A. (2009). Soliton model of competitive neural dynamics during binocular rivalry, *Phys Rev Lett, 102*, 258701.

29. Moreno-Bote, R., Rinzel, J. & Rubin, N. (2007) Noise-induced alternations in an attractor network model of perceptual bistability, *J. Neurophysiol., 98*, 1125–1139.

30. Pinto, D. J. & Ermentrout, G. B. (2001). Spatially structured activity in synaptically coupled neuronal networks: I. Traveling fronts and pulses, *SIAM J Appl Math, 62*, 206–228.

31. Sandstede, B. (2007). Evans functions and nonlinear stability of traveling waves in neuronal network models *Int. J. Bif. Chaos, 17*, 2693–2704

32. Shpiro, A., Curtu, R., Rinzel, J. & Rubin, N. (2007). Dynamical characteristics common to neuronal competition models, *J Neurophysiol, 97*, 462–73.

33. Shpiro, A., Moreno-Bote, R., Rubin, N.R. & Rinzel, J. (2009). Balance between noise and adaptation in competition models of perceptual bistability, *J Comp. Neurosci., 27*, 37–54.

34. Skinner, F. K. , Kopell, N. & Marder, E. (1994). Mechanisms for oscillation and frequency control in reciprocally inhibitory model neural networks, *J Comput. Neurosci., 1*, 69–87.

35. Sincich, L. & Blasdel, G. G. (2001). Oriented axon projections in primary visual cortex of the monkey., *J Neurosci, 21*, 4416–4426.

36. Tabak, J., Senn, W., O'Donovan, M. J. & Rinzel, J. (2000) Modeling of spontaneous activity in developing spinal cord using activity-dependent depression in an excitatory network, *J Neurosci., 20*, 3041–3056.

37. Taylor, A. L., Cottrell, G. W. & Kristan, W. B., Analysis of oscillations in a reciprocally inhibitory network with synaptic depression, *Neural Computation, 14*, 561–81.

38. Tootell, R. B. , Switkes, E., Silverman, M. S. & Hamilton, S. L. (1988). Functional anatomy of macaque striate cortex. II. Retinotopic organization, *J Neurosci., 8*, 1531–1568.

39. Tsodyks, M., Pawelzik, K. & Markram, H. (1998). Neural networks with dynamic synapses, *Neural Comput., 10*, 821–835.

40. Varela, J. A. , Sen, K., Gibson, J., Fost, J., Abbott, L. F. & Nelson, S. B. (1997). A quantitative description of short-term plasticity at excitatory synapses in layer 2/3 of rat primary visual cortex, *J Neurosci, 17*, 7926–40.

41. Wilson, H. R. , Blake, R. & Lee, S. H. (2001). Dynamics of traveling waves in visual perception, *Nature, 412*, 907–10.

42. Zhang, L. (2003). On stability of traveling wave solutions in synaptically coupled neuronal networks. *Differential Integral Eqs, 16*, 513–536.

RECENT REPORTS

53/11	Surface growth kinematics via local curve evolution	Moulton Goriely
54/11	A multiple scales approach to evaporation induced Marangoni convection	Hennessey Münch
55/11	The dynamics of bistable liquid crystal wells	Luo Majumdar Erban
56/11	Real-Time Fluid Effects on Surfaces using the Closest Point Method	Auer Macdonald Treib Schneider Westermann
57/11	Isolating intrinsic noise sources in a stochastic genetic switch	Newby
58/11	Riemann-Cartan Geometry of Nonlinear Dislocation Mechanics	Yavari Goriely
59/11	Helices through 3 or 4 points?	Goriely Neukirch Hausrath
60/11	Bayesian data assimilation in shape registration	Cotter Cotter Vialard
61/11	Asymptotic solution of a model for bilayer organic diodes and solar cells	Richardson Please Kirkpatrick

Copies of these, and any other OCCAM reports can be obtained from:

Oxford Centre for Collaborative Applied Mathematics
Mathematical Institute
24 - 29 St Giles'
Oxford
OX1 3LB
England
www.maths.ox.ac.uk/occam